The Avaatech XRF Core Scanner: technical description and applications to NE Atlantic sediments

THOMAS O. RICHTER[1], SJERRY VAN DER GAAST[1], BOB KOSTER[2], AAD VAARS[3], RINEKE GIELES[1], HENKO C. DE STIGTER[1], HENK DE HAAS[1] & TJEERD C. E. VAN WEERING[1]

[1]*Department of Marine Chemistry and Geology, Royal Netherlands Institute for Sea Research (NIOZ), P.O. Box 59, 1790 AB Den Burg, The Netherlands (e-mail: thomasr@nioz.nl)*

[2]*Department of Marine Technology, Royal Netherlands Institute for Sea Research (NIOZ), P.O. Box 59, 1790 AB Den Burg, The Netherlands*

[3]*Avaatech Analytical X-Ray Technology, Wagenmakerstraat 11, 1791 EJ Den Burg, The Netherlands*

Abstract: X-ray fluorescence (XRF) core scanning provides rapid high-resolution (down to 1 mm) records of chemical composition on split sediment cores. The measurements are non-destructive and require very limited sample preparation. The new Avaatech XRF Core Scanner, operational since 2002, covers the atomic mass range from Al to U. Instrument parameters, especially tube voltage, can be adjusted to provide optimum settings for selected elements or sets thereof. Owing to the nature of the surface of split sediment cores, particularly effects resulting from sample inhomogeneity and surface roughness, results are semi-quantitative, yet provide reliable records of the relative variability in elemental composition downcore. Selected case studies from diverse sedimentary settings in the NE Atlantic Ocean illustrate a range of applications of XRF logging data. These include preliminary stratigraphic interpretations (glacial–interglacial cycles), provenance studies of the terrigenous sediment fraction, lithological characterization, early diagenetic processes and distinction between carbonate phases (aragonite v. calcite).

Various logging methods, mostly dealing with physical sediment properties, are presently widely used to produce high-resolution or quasi-continuous records for rapid, non-destructive characterization of marine and lacustrine sediment sequences (e.g. Weaver & Schultheiss 1990; Zolitschka *et al.* 2001). These measurements, frequently performed shortly after core retrieval during research cruises or field campaigns, can already provide preliminary stratigraphic information. More generally, they represent a first means of assessing the quality of sedimentary records and provide constraints on sampling strategies for subsequent analysis on discrete samples, commonly at lower resolution and/or over selected core intervals.

X-ray fluorescence (XRF) logging was first developed at The Netherlands Institute for Sea Research (NIOZ) in 1988 (Jansen *et al.* 1998). An updated version of this CORTEX scanner was delivered to the University of Bremen in 1997, and the second-generation Avaatech XRF Core Scanner (ACS) has been operational since 2002 at NIOZ and University of Bremen. XRF core scanning essentially tracks downcore changes in chemical composition (major, minor and trace elements). By contrast, most other logging data (e.g. magnetic susceptibility, gamma-ray attenuation, seismic velocity, sediment colour) usually depend on a combination of sediment parameters, such as grain-size changes combined with changes in the ratio of terrigenous v. biogenic components (e.g. Bassinot 1993; Weber *et al.* 1997). Applications of XRF core scanning include, among others, initial correlation between cores, preliminary stratigraphic interpretations including astronomical tuning of sedimentary sequences (e.g. Norris & Röhl 1999; Pälike *et al.* 2001), investigating terrigenous input patterns and provenance of terrigenous material (e.g. Haug *et al.* 2001; Lamy *et al.* 2004), tracing early diagenetic processes (Funk *et al.* 2004) and recognition of sedimentological events by specific lithologies (e.g. turbidites, sapropels, ash layers).

In this contribution, we first provide a technical description of the XRF logging system, including recent developments and improvements of the new Avaatech XRF Core Scanner (http://www.avaatech.com). Then, we discuss

From: ROTHWELL, R.G. 2006. *New Techniques in Sediment Core Analysis*. Geological Society, London, Special Publications, **267**, 39–50. 0305-8719/06/$15.00

applications of XRF core scanning based on case studies from the NE Atlantic Ocean.

X-ray fluorescence (XRF) logging

The principle of X-ray fluorescence is discussed by Jenkins & De Vries (1970). Briefly, under the influence of incoming X-ray radiation an electron is ejected from an inner shell of an atom. The resulting vacancy is subsequently filled by an electron falling back from an outer shell, and the energy difference between both shells is emitted as electromagnetic radiation. The wavelength(s) of emitted radiation are characteristic for each element, and the amplitudes of peaks in the XRF spectrum are proportional to the concentration of corresponding elements in the analysed sample.

Set-up of XRF logging system and comparison of CORTEX (1988, 1997) and Avaatech (2002) scanners

The CORTEX and Avaatech scanners perform continuous downcore XRF analysis on the surface of split sediment cores. Technical details for both scanners are presented in Table 1. Both instruments are installed in sea-going containers and can thus be used onboard research vessels. The basic instrument set-up is virtually identical for both scanners (Figs 1 & 2). A prism is lowered onto the sediment surface at each measurement position, and incoming radiation generated in the X-ray tube enters at an angle of 45°. The length of the X-ray beam (in downcore direction) is determined by a horizontally mounted variable slit system below the X-ray tube, the width of the beam is fixed at 12 or 16 mm, respectively (Table 1). The detector for outgoing radiation is likewise installed at an angle of 45°. The entire measurement system is flushed with helium to prevent partial or complete absorption of emitted soft radiation from the sample by air. With a net counting time of 30 s as commonly applied, each individual multi-element analysis takes approximately 1 min. For exploratory analysis of major elements only, reliable count statistics can be achieved with lower counting times. For example, 1 m of sediment can be logged for Ca and Fe to obtain a preliminary stratigraphy of marine sediments (cf. below) in 15–20 min (2 cm resolution, counting time 10 s).

In the CORTEX scanner, split core halves are transported along the measurement system. In the Avaatech instrument the measurement system instead moves along the half core, thus reducing the overall instrument size. The Avaatech XRF Core Scanner allows for a larger atomic weight range of elements to be analysed (Table 1). This was made possible because measurement conditions, especially tube voltage, can be varied to obtain optimal settings for specific elements or sets thereof (Table 2). Filters can be placed in the incident beam to attenuate part of the hard radiation from the X-ray tube spectrum, thus improving sensitivity for a range of elements of interest. Detection limits of elements in the atomic mass range K–Sr are also significantly lower for the Avaatech scanner compared to the earlier CORTEX system (Table 3).

Samples and sample preparation

For X-ray fluorescence analysis with conventional laboratory instruments, samples need to be homogenous, dry, and have a flat and smooth surface. Split sediment cores do not meet these requirements. The water content generally ranges from 30 to 70% in the uppermost metres of marine sediments, with a rapid decrease immediately below the sediment surface. Effects of sample inhomogeneity and surface roughness are particularly pronounced for sediments containing abundant

Table 1. *Technical details of CORTEX and Avaatech XRF scanners*

	CORTEX (1988, 1997)	Avaatech (2002)
X-ray tube	KEVEX	Oxford
Target X-ray tube	Mo	Rh
Film of measuring cell	Mylar 4 μm	Ultralene 4 μm
Film on sample	Polypropylene 100 μm	Ultralene 4 μm
Irradiated sample dimensions	L = 10 mm, W = 12 mm	L = 0.5–10 mm, W = 16 mm
Detector	Energy dispersive, KEVEX SuperDry Si(Li), Peltier cooled	Energy dispersive, AMPTEK Si-PIN, Peltier cooled
Window of detector	Be 10 μm	Be 13 μm
Elements analysed (atomic weight range)	K–Sr	Al–U
Processing software of measured spectra	KEVEX	CANBERRA
Accuracy along the *X*-axis of the scanner	not determined	±0.035 mm

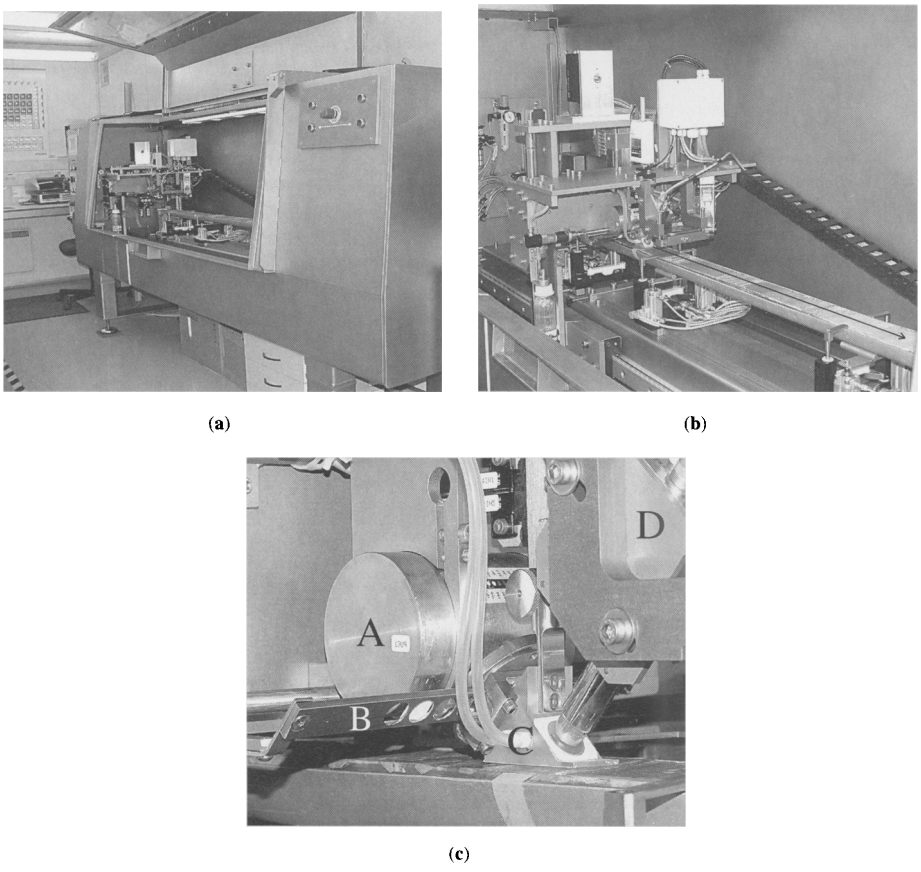

Fig. 1. Views of the Avaatech XRF Core Scanner. (**a**) General overview of the instrument. (**b**) Measurements on a split sediment core. Arrow on core surface depicts the (stepwise) movement of the measurement system along the core surface. (**c**) Detailed view of the X-ray tube (A), filters that can be placed in the incoming X-ray beam (B), prism lowered onto the sediment surface covered with Ultralene film (C) and XRF detector (D).

medium–coarse sand-sized particles such as shell fragments in coastal environments or foraminifera and ice-rafted grains in deep-sea settings, but are less significant in most fine-grained marine sediments.

Sample preparation includes careful flattening of the sediment surface to remove irregularities from core slicing. The sediment surface is subsequently covered with thin (4 μm) Ultralene film, further diminishing surface roughness and

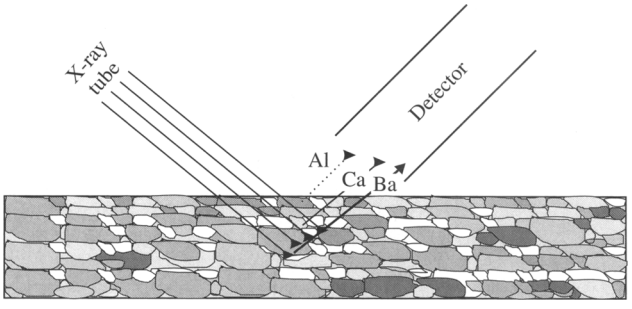

Fig. 2. Simplified diagram showing principle of XRF logging on split sediment cores and response depth (not to scale) of selected elements to incoming X-ray radiation (see text).

Table 2. *Instrumental settings of the Avaatech XRF Core Scanner for specific sets of elements*

Tube voltage (kV)	Filter	Elements analysed
5	none	(Mg), Al*, Si*
10	none	Al, Si, P, S, Cl, K, Ca, Ti, Mn, Fe, Cu, Zn
30	Pd thick	Br, Rb, Sr, Zr
50	Cu	Ba, Pb, U

* At low bulk concentrations or for higher accuracy.

preventing contamination of the prism unit during core logging.

The poor quality of samples used for XRF logging, compared to fused beads or powder pellets of conventional laboratory X-ray fluorescence, necessarily means that XRF logging data are only semi-quantitative. However, the very limited sample preparation and rapid analysis allow for high sample throughput, and XRF logging records faithfully trace *relative* downcore variations in the elemental composition of sediments.

Response depth to incoming X-ray radiation and element detection limits

The response depth of elements to incoming X-ray radiation is dependent on the wavelength of emitted radiation, itself related to atomic weight, and on the chemical composition of the matrix (Jenkins & De Vries 1970). For average marine sediments with significant amounts of Si, Al and/or Ca and some Fe, the maximum detection depth for Ba (emitted wavelength 32.2 keV) is 2–4 mm. For lighter elements, the detection depth is progressively smaller, for example 1–2 mm for Sr (14.2 keV), 1 mm for Fe (6.4 keV), 0.5 mm for Ca (3.7 keV) and 0.05 mm for Al (1.5 keV). Consequently, the detection limit for various elements also, to a first approximation, decreases with increasing atomic weight (Table 3). For heavy elements, such as Zr and Ba, the detection limit again increases because the XRF detector is slightly less efficient at the high wavelengths of their emitted radiation.

Spatial resolution

The irradiated sample length (ISL) of the Avaatech XRF Core Scanner can be varied between 0.5 and 10 mm. Generally, a maximum resolution of 1 mm is recommended in order to maintain sufficient analytical volume (sample volume from which emitted X-rays are detected) for reliable count statistics. Further, the effects of sample inhomogeneity and surface roughness become increasingly important at higher spatial resolution, resulting in more strongly fluctuating X-ray intensities between adjacent samples and a lower signal-to-noise ratio. In fine-grained clayey sediments, these effects are less pronounced to negligible, and an ISL and spatial resolution of 0.5 mm may be applied.

For heavy elements (e.g. Sr, Ba) interaction of their emitted radiation with (lighter) elements present in the sample matrix will result in the XRF signal effectively being derived from a larger area in downcore (and crosscore) direction, hence decreasing the true spatial resolution. Thus, a step size and ISL of 3 and 2 mm for Ba and Sr, respectively, is generally sufficient, as

Table 3. *Detection limits of the CORTEX and Avaatech XRF core scanners (selected elements)*

Element	Atomic weight	Kα line (keV)	Detection limit (ppm)	
			CORTEX	Avaatech
Mg	24	1.25	n.a.	20000
Al	27	1.49	n.a.	2000
Si	28	1.74	n.a.	1000
P	31	2.01	n.a.	500
S	32	2.31	n.a.	500
K	39	3.31	2000	400
Ca	40	3.69	800	200
Ti	48	4.51	1200	500
Mn	55	5.89	1400	100
Fe	56	6.40	210	45
Sr	88	14.14	260	5
Zr	91	15.74	n.a.	20
Ba	137	32.19	n.a.	40
Pb	207	10.84 (Lα)	n.a.	10

n.a., not applicable

Table 4. *Locations and settings of sediments cores, and origin of XRF records*

Core	Latitude	Longitude	Water depth (m)	Setting	Elements shown	Instrument
MD992282	59°29′N	10°34′W	1360	Seamount	Ca, Fe	CORTEX
ENAM9606	55°39′N	13°59′W	2543	Sediment drift	Ca	CORTEX
ENAM9321	62°44′N	4°0′W	1020	Sediment drift	K, Ti	CORTEX
STRAT01-06	62°42′N	1°16′W	1576	Mud volcano	Ca, Si, Al, Fe, Mn, S	Avaatech
M2001-05	53°12′N	14°49′W	840	Carbonate mound	Ca, Fe, Sr	Avaatech
ENAM9706	53°12′N	15°05′W	2131	Continental margin	Ca, Sr	Avaatech

measurements at higher resolution will not provide additional information on the downcore variability of these elements.

Applications to NE Atlantic sediments

Examples from NE Atlantic sediments, covering various timescales and diverse sedimentary settings, serve to illustrate a wide range of applications of XRF core scanning (Table 4, Fig. 3). We focus on preliminary conclusions that can be derived from XRF logging data alone or in combination with other non-destructive shipboard datasets (e.g. magnetic susceptibility records, lithological description). As the XRF records shown below were obtained partly with the CORTEX (1988) instrument and partly with the Avaatech Core Scanner, absolute element count rates are not directly comparable between all records.

Ca (carbonate) records: Milankovitch and sub-Milankovitch variability

It is well established that calcium carbonate records in the Atlantic Ocean can be related to glacial–interglacial cycles, with higher carbonate concentrations during interglacial periods (Kennett 1982; Balsam & McCoy 1987). Hence, preliminary stratigraphic interpretations can be based on downcore XRF records of Ca and Fe, tracing fluctuations in the relative abundance of biogenic carbonate and terrigenous material, respectively.

Core MD992282 from the southern flank of Rosemary Bank seamount contains 34.35 m of alternating light-coloured silty sand and darker-coloured silty clay. The XRF record (Fig. 4) displays recurrent antiphase oscillations of Ca and Fe, with higher Ca count rates corresponding to coarser-grained light-coloured sediments.

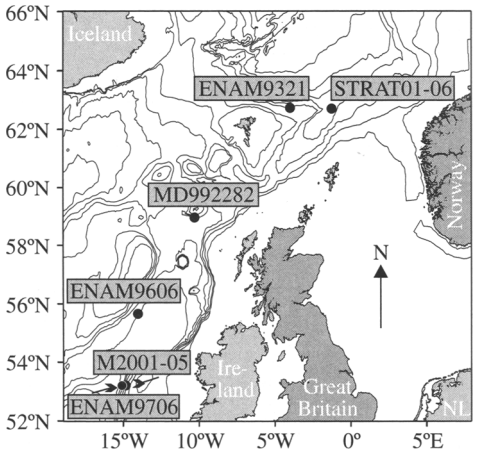

Fig. 3. Simplified bathymetry of the NE Atlantic Ocean showing locations of sediment cores used in this study.

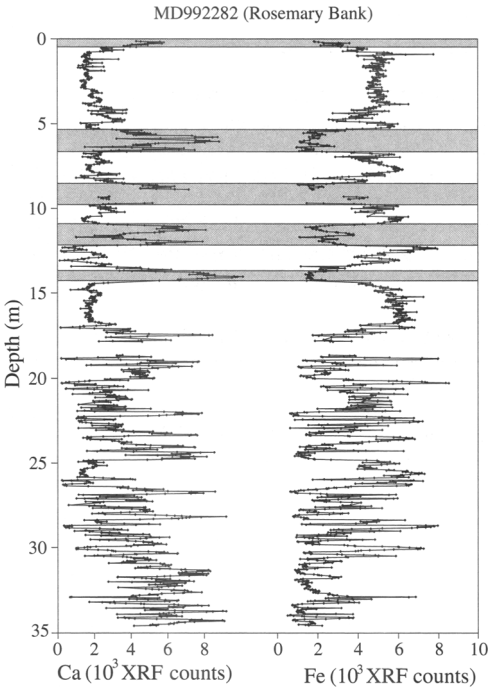

Fig. 4. Ca and Fe count rates for core MD992282 (Rosemary Bank) showing glacial–interglacial variability. Shaded rectangles in upper part of figure indicate interglacial intervals (light-coloured sediments, high Ca, low Fe). Data gaps are due to (partial) voids in sediment sections.

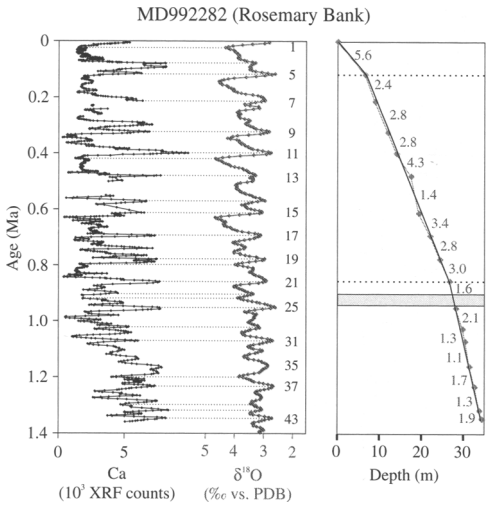

Fig. 5. Left panel: tentative correlation of MD992282 Ca record with smoothed and spliced benthic oxygen isotope record from Feni Drift ODP sites 980/981 (Raymo *et al.* 2004 and references therein). Stippled lines indicate tie points between both records. Numbers next to oxygen isotope records represent selected interglacial isotope stages. Right panel: resulting age model. The thick black line represents the general age–depth relation; stippled horizontal lines depict upcore increases in mean long-term sedimentation rate. The grey line indicates the age–depth relation for individual glacial–interglacial cycles. Numbers are sedimentation rates (cm ka^{-1}) between peak interglacial oxygen isotope events (grey diamonds). The shaded rectangle corresponds to an increase in ice volume-related mean $\delta^{18}O$ (transition midpoint: 922 ± 12 ka, duration 40 ± 9 ka, after Mudelsee & Schulz 1997).

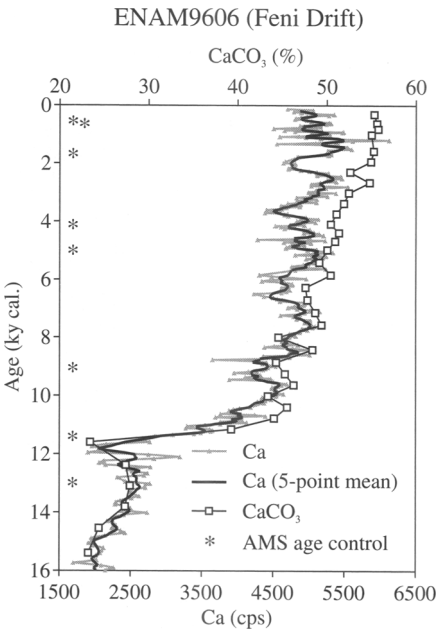

Fig. 6. Ca count rates and $CaCO_3$ concentrations from Feni Drift core ENAM9606.

Downcore, an obvious shift towards higher-frequency variability in the depth domain occurs below approximately 18 m core depth. Figure 5 illustrates the tentative correlation between the record of Ca count rates and a record of benthic oxygen isotopes (Raymo *et al.* 2004 and references therein) from the nearby Feni Drift (ODP sites 980 and 981) tracing global ice-volume fluctuations over the last 1.4 Ma. According to this stratigraphic scheme, the shift in the character of the XRF record around 18 m core depth corresponds to the Mid-Pleistocene transition from predominantly 41 ka cyclicities of global ice volume in the lower Pleistocene to larger mean global ice volume and pronounced 100 ka cycles in the upper Pleistocene. The exceptional character of Marine Isotope Stage 11 (highest Ca count rates of entire XRF record) is consistent with growing evidence for the unusual nature of this interglacial period (e.g. Howard 1997).

Average sedimentation rates for successive glacial–interglacial cycles show a two-step increase upcore. The first increase closely coincides with an increase in ice-volume-related mean $\delta^{18}O$ between 940 and 900 ka BP (Mudelsee & Schulz 1997), suggesting a coeval change in depositional conditions possibly related to changing average current regimes. The second increase towards distinctly higher sedimentation rates during the last glacial cycle could represent an artefact of core stretching, as commonly observed in the uppermost metres of giant piston cores (Széréméta *et al.* 2004).

A high-resolution record from Feni Drift, sediment core ENAM9606, provides evidence for carbonate variability on sub-Milankovitch timescales (Fig. 6). Following a rapid increase in Ca count rates during the later part of Termination I (12–10 ka), a further slight increase spanning nearly the entire Holocene is punctuated by pronounced cyclic variability. The XRF record shows generally good agreement with a lower-resolution carbonate record based on discrete samples. The apparently increasing difference between both records in the late Holocene is ascribed to the higher water content of near-surface sediments. Holocene carbonate variability may be related to variable dilution by bottom-current-transported terrigenous material

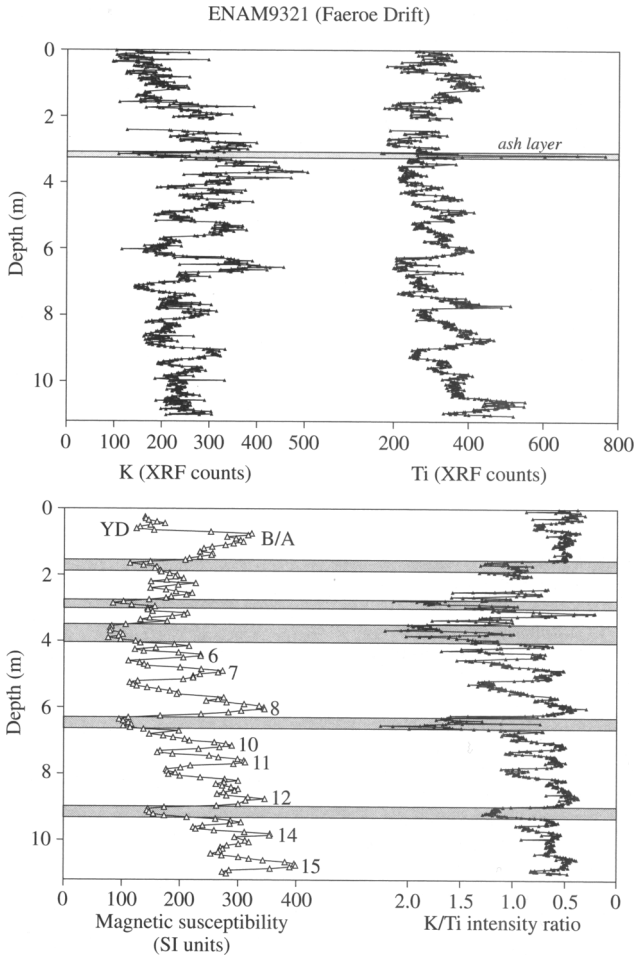

Fig. 7. XRF and magnetic susceptibility records for Faeroe Drift core ENAM9321. Stratigraphy after (Rasmussen *et al.* 1996, 1998). Shaded rectangles correspond to Heinrich events 1–5; numbers represent selected ice-core interstadials; B/A, Bølling–Allerød; YD, Younger Dryas.

(e.g. Chapman & Shackleton 2000) and/or to fluctuating carbonate productivity. The nature of this centennial- to millennial-scale variability and possible forcing mechanisms will be fully discussed elsewhere.

Provenance of terrigenous material and Dansgaard–Oeschger cycles

Millennial-scale climate variability during the last glacial cycle was initially deduced from Greenland ice-core records (Dansgaard *et al.* 1993). Correlative variations were first described for marine sediments from the Faeroe Margin (Rasmussen *et al.* 1996), and subsequently in a growing number of marine and terrestrial palaeoclimate records worldwide (Voelker & Workshop Participants 2002). These Dansgaard–Oeschger cycles are characterized by recurrent shifts in North Atlantic deep-circulation patterns. Magnetic susceptibility records indicate enhanced deposition of magnetic minerals by bottom currents during interstadial (warm) events, and reduced bottom-current activity during stadial (cold) periods and Heinrich events (Rasmussen *et al.* 1996; Kissel *et al.* 1999).

Following some earlier evidence based on clay mineral assemblages and quantitative chemical analysis (e.g. Blamart *et al.* 1999; Rasmussen *et al.* 1998), we show here (Fig. 7) that the Dansgaard–Oeschger cycles in Faeroe Margin sediments are also accompanied by repetitive shifts in the composition of the terrigenous fraction.

Potassium and titanium can be dominantly linked to acidic (average continental crust) and basaltic sources, respectively. The XRF intensity ratio of these elements (K/Ti), tracing the relative importance of both terrigenous sources, shows a systematic relationship with magnetic susceptibility which was itself previously correlated to the Greenland ice-core record. This implies enhanced deposition of bottom-current-transported basaltic material derived from the North Atlantic volcanic province during interstadial periods (low K/Ti), and an increased contribution of continentally derived material, possibly through ice rafting from Fennoscandia, during stadial periods and, especially, Heinrich events.

Mud volcano sediments at the Faeroe–Shetland Margin: lithological characterization and early diagenetic processes

Core STRAT01-06 was taken in the northern Faeroe–Shetland Channel on top of a mud volcano, which forms part of a group of relatively small structures rising several tens of metres above the surrounding seabed (Long *et al.* 2003). It contains two lithological units separated by a sharp boundary at 260 cm core depth. The lower unit, characterized by numerous mm- to cm-scale clasts embedded in a fine-grained matrix, is interpreted as being related to mud volcano activity. The overlying upper unit is similar to typical hemipelagic sediments in the wider study area.

These two units are clearly distinguished on the XRF logging and magnetic susceptibility records (Fig. 8). The upper unit shows cyclic fluctuations of magnetic susceptibility consistent with the regional pattern during the last glacial period (compare with Fig. 7), the record of Ca count rates depicts a thin (*c.* 3 cm) Holocene section at the core top. The boundary with the underlying mud volcano unit shows an approximately 10-fold decrease in both magnetic susceptibility and Ca count rates, with consistently low values for both parameters in underlying sediments. The mud volcano deposits can be divided into two subunits based on a second magnetic susceptibility decrease at approximately 540 cm core depth. The lower mud volcano unit contains occasional mm-sized light-coloured limestone clasts, which cause sharp short-lived maxima of Ca count rates in the XRF record. While Si count rates remain comparatively constant across the lithological boundary, the relationship between Si and Al indicates different sources of silicon for the

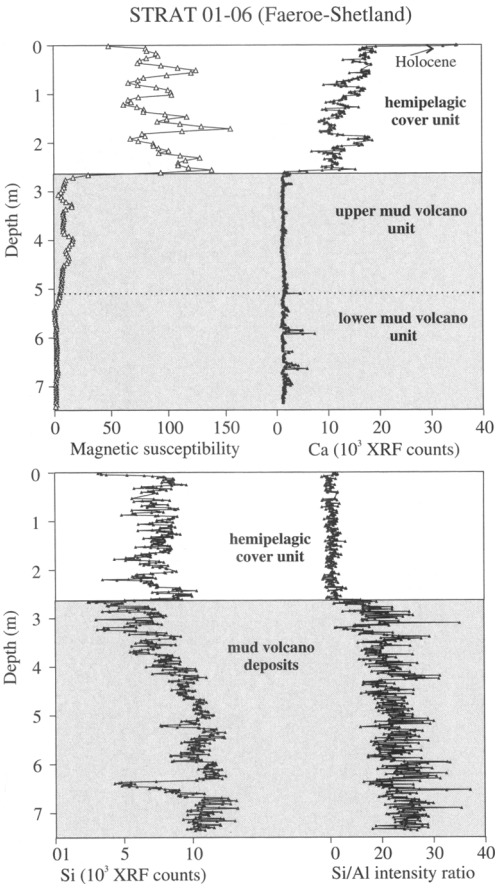

Fig. 8. Magnetic susceptibility and XRF records from core STRAT01-06 (Faeroe–Shetland margin) showing the sharp lithological boundary between mud volcano deposits and overlying hemipelagic sediments.

mud volcano deposits and hemipelagic cover sediments (Fig. 8). Fairly constant Si/Al-ratios in the hemipelagic unit imply that Si is mainly derived from terrigenous aluminosilicates, whereas higher and more variable ratios in mud volcano deposits suggest a significant contribution from biogenic opal.

Count rates of Fe, Mn and S trace early diagenetic processes within the mud volcano unit (Fig. 9). Sulphur count rates show two abrupt downcore increases at 260 and 330 cm core depth. The first increase coincides with the main lithological boundary, whereas the second increase seems to mark the limit between oxidizing and reducing conditions within the mud volcano unit. The oxidized upper part shows three sharp maxima in Fe count rates and a pronounced double Mn peak, all of which are interpreted as

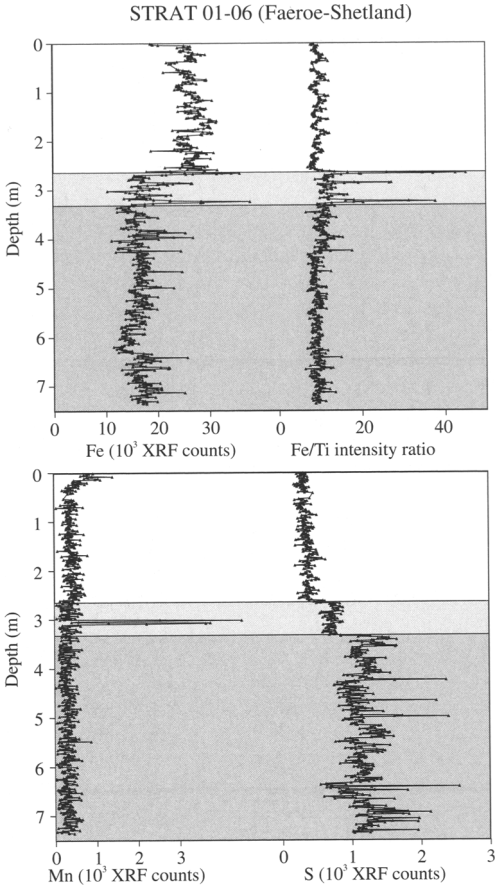

Fig. 9. XRF records from core STRAT01-06 to illustrate early diagenetic processes within mud volcano deposits. Shading indicates oxidized top of mud volcano unit (light grey pattern) and underlying reducing environment (dark grey pattern).

palaeo-oxidation fronts. The diagenetic origin of the Fe spikes is confirmed by sharp increases in the Fe/Ti ratio. While Fe and Ti are closely related to each other in the terrigenous fraction, Fe is (partly) prone to diagenetic remobilization in pore waters, whereas Ti is inert to diagenetic processes. The reduced lower part of the mud volcano unit displays numerous short-lived maxima of S count rates, consistently accompanied by concomitant Fe maxima, implying precipitation of pyrite or other Fe-sulphide phases within reducing microenvironments.

The conclusions discussed above are also illustrated by element cross-plots (Fig. 10). The plot of Si v. Al demonstrates that data from the two lithological units plot in different fields, consistent with different sources of silicon (cf. above). In the plot of Fe v. S (only data from lower unit shown) there is little relationship between both elements for most data points where Fe is presumably of terrigenous origin. On the other hand, diagenetic Fe enrichments fall outside the main cluster of data points, and Fe-oxide and Fe-sulphide phases can be easily distinguished based on S count rates.

Cold-water carbonate mounds: detection of hardgrounds and coralline aragonite

Cold-water carbonate mounds with deep-water corals (mainly *Lophelia pertusa* and *Madrepora oculata*) are widespread along both margins of Rockall Trough in the NE Atlantic Ocean, rising up to about 350 m above the surrounding sea floor (e.g. de Mol *et al.* 2002, Kenyon *et al.* 2003, van Weering *et al.* 2003). Here we present results from piston core M2001-05, which was taken on the lower flank of a mound within a mound cluster on SE Rockall Trough margin.

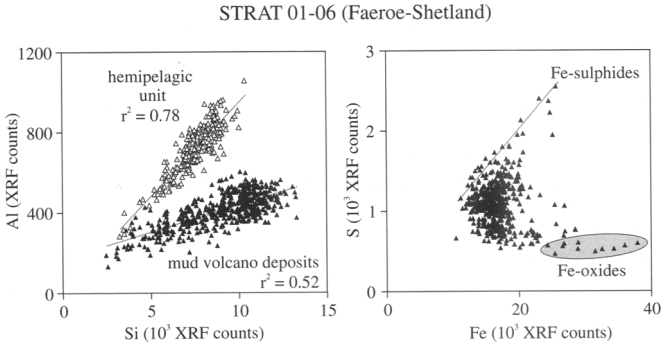

Fig. 10. Diagnostic element cross-plots from core STRAT01-06 showing lithological characterization (left panel) and different sources of iron in the mud volcano deposits (right panel).

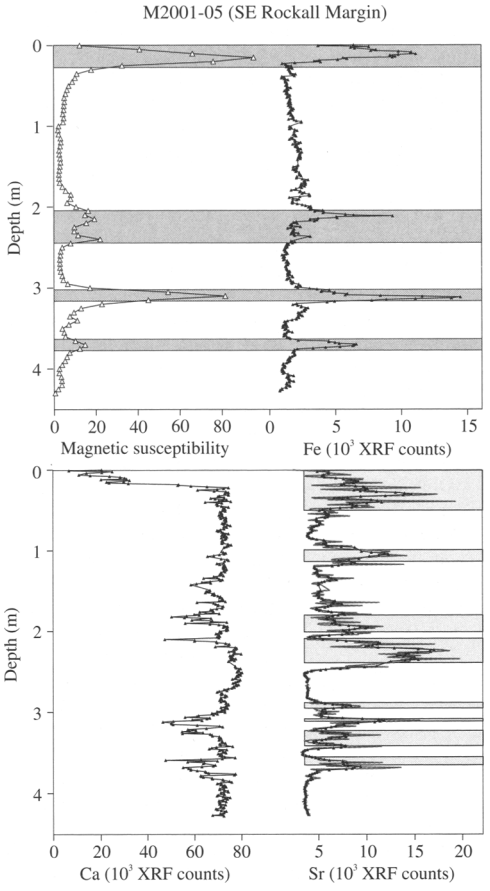

Fig. 11. Magnetic susceptibility and XRF records from cold-water carbonate mound core M2001-05 (SE Rockall Margin). Shaded rectangles in the upper panel indicate hardgrounds with enhanced terrigenous input. The line with symbols in the lower right panel represents a five-point running mean of Sr count rates; the thin grey line corresponds to raw data. Shaded rectangles indicate core intervals containing fragments of cold-water corals.

This core consists dominantly of cemented foraminiferal sands with intercalated hardgrounds. Numerous core intervals contain fragments of cold-water corals, presumably reflecting temporal variability of coral growth and/or variable preservation of coralline aragonite.

Magnetic susceptibility and XRF records are shown in Figure 11. Calcium count rates are high throughout the sediment record (excluding the top 20 cm), consistent with the dominant lithology. The scatter in the Ca record can be largely ascribed to increased surface roughness and scattering effects from large particles in sandy sediments. Hardgrounds display sharp maxima of magnetic susceptibility and Fe count rates. They are also characterized by high count rates of numerous other terrigenous elements (not shown). Compared to the Ca record, Sr count rates are highly variable; sediment intervals with coral fragments consistently have higher Sr count rates than over- and underlying intervals.

Hence, Sr count rates in this setting serve to distinguish between foraminiferal calcite and coralline aragonite, the latter carbonate phase containing significantly higher percentages of Sr. This is further illustrated by the XRF records from a nearby pelagic reference core (Fig. 12), where Ca and Sr show largely consistent patterns of variability over several glacial–interglacial cycles. Maximum Sr count rates in the carbonate mound record are at least twice as high as those in the pelagic reference core.

Concluding remarks

X-ray fluorescence core scanning provides high-resolution (quasi-continuous) palaeoenvironmental information in a variety of sedimentary settings. While the results are inherently semi-quantitative due to the nature of the surface of split-sediment cores (particularly due to effects of sample inhomogeneity and surface roughness),

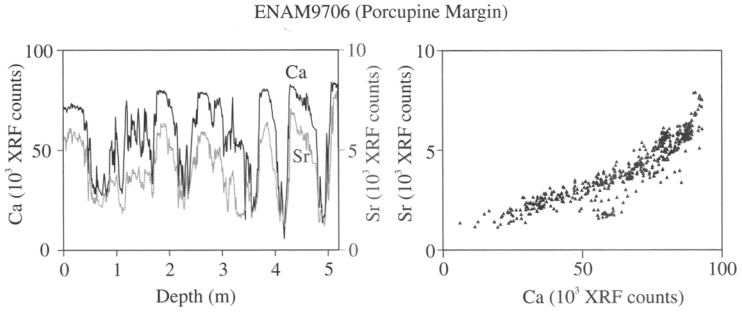

Fig. 12. XRF records (Ca and Sr) from Porcupine Margin core ENAM9706 (pelagic reference site for carbonate mound core M2001-05).

XRF logging records faithfully trace *relative* downcore variability in the elemental composition of sediments. As the instrument is installed in a sea-going container, results can potentially be obtained onboard research vessels within hours after core retrieval and can be used to adapt ongoing sampling programmes. The measurements are non-destructive and can provide constraints on sampling strategies for subsequent analysis on discrete samples.

XRF logging results can be interpreted in combination with other non-destructive (shipboard) data such as magnetic susceptibility records and lithological description. Cross-elemental plots and element intensity ratios can be applied to enhance the signal-to-noise ratio, because – to a first approximation – variable surface roughness effects (for example, related to downcore grain-size variability) will affect XRF count rates for all elements in a similar way. Inter-element relationships can also be helpful to distinguish between multiple sources for some elements and provide clues on sediment mineralogy. For example, combined distribution patterns of Si and Al trace the relative contributions of aluminosilicates v. biogenic opal to total sedimentary silicon. The coupled use of Fe, Ti and S can differentiate between a dominantly terrigenous supply of iron and distinct early diagenetic iron enrichments in oxidizing and reducing environments. Sr and Ca distribution patterns taken together define the relative importance of aragonite (high Sr) v. calcite (low Sr).

We thank K.-C. Emeis, one anonymous reviewer and the editor, G. Rothwell, for evaluating the manuscript.

References

Balsam, W.L. & McCoy, F.W., Jr. 1987. Atlantic sediments: Glacial/interglacial comparisons. *Paleoceanography*, **2**, 531–542.

Bassinot, F. 1993. Sonostratigraphy of tropical Indian Ocean giant piston cores: toward a rapid and high-resolution tool for tracking dissolution cycles in Pleistocene carbonate sediments. *Earth and Planetary Science Letters*, **120**, 327–344.

Blamart, D., Balbon, E., Kissel, C., Turpin, L., Robin, E., Labeyrie, L. & Deconinck, J.-F. 1999. Deep water circulation variability in the southern Norwegian Sea during the last glacial period. *Terra Abstracts*, **4**, 164.

Chapman, M.R. & Shackleton, N.J. 2000. Evidence of 550-year and 1000-year cyclicities in North Atlantic circulation patterns during the Holocene. *The Holocene*, **10**, 287–291.

Dansgaard, W., Johnsen, S.J. *et al.* 1993. Evidence for general instability of past climate from a 250-kyr ice record. *Nature*, **364**, 218–220.

de Mol, B., van Rensbergen, P. *et al.* 2002. Large deep-water coral banks in the Porcupine Basin, southwest Ireland. *Marine Geology*, **188**, 193–231.

Funk, J.A., von Dobeneck, T. & Reitz, A. 2004. Integrated rock magnetic and geochemical quantification of redoxomorphic iron mineral diagenesis in Late Quaternary sediments from the equatorial Atlantic. *In*: Wefer, G., Mulitza, S. & Ratmeyer, V. (eds) *The South Atlantic in the Late Quaternary: Reconstruction of Material Budgets and Current Systems*. Springer, Berlin, 237–260.

Haug, G.H., Hughen, K.A., Sigman, D.M., Peterson, L.C. & Röhl, U. 2001. Southward migration of the Intertropical Convergence Zone through the Holocene. *Science*, **293**, 1304–1308.

Howard, W.R. 1997. A warm future in the past. *Nature*, **388**, 418–419.

Jansen, J.H.F., Van der Gaast, S.J., Koster, B. & Vaars, A. 1998. CORTEX, a shipboard XRF-scanner for element analyses in split sediment cores. *Marine Geology*, **151**, 143–153.

Jenkins, R. & De Vries, J.L. 1970. *Practical X-ray Spectrometry*. Macmillan, London.

Kennett, J.P. 1982. *Marine Geology*. Prentice-Hall, Eaglewood Cliffs, NJ.

Kenyon, N.H., Akhmetzhanov, A.M., Wheeler, J.W., van Weering, T.C.E., de Haas, H. & Ivanov, M.K. 2003. Giant carbonate mud mounds in the southern Rockall Trough. *Marine Geology*, **195**, 5–30.

Kissel, C., Laj, C., Labeyrie, L., Dokken, T., Voelker, A. & Blamart, D. 1999. Rapid climatic variations during marine isotopic stage 3: magnetic analysis of sediments from Nordic seas and North Atlantic. *Earth and Planetary Science Letters*, **171**, 489–502.

Lamy, F., Kaiser, J., Ninnemann, U., Hebbeln, D., Arz, H.W. & Stoner, J. 2004. Antarctic timing of surface water changes off Chile and Patagonian ice-sheet response. *Science*, **304**, 1959–1962.

Long, D., Hoult, R. *et al.* 2003. Mud mound/?diapiric features in the Faroe–Shetland Channel. *Geophysical Research Abstracts*, **5**, 11201.

Mudelsee, M. & Schulz, M. 1997. The Mid-Pleistocene climate transition: onset of 100 ka cycle lags ice volume build-up by 280 ka. *Earth and Planetary Science Letters*, **151**, 117–123.

Norris, R.D. & Röhl, U. 1999. Carbon cycling and chronology of climate warming during the Palaeocene/Eocene transition. *Nature*, **401**, 775–778.

Pälike, H., Shackleton, N.J. & Röhl U. 2001. Astronomical forcing on late Eocene marine sediments. *Earth and Planetary Science Letters*, **193**, 589–602.

Rasmussen, T.L., Thomsen, E. & van Weering, T.C.E. 1998. Cyclic sedimentation on the Faeroe drift 53-10 ka BP related to climatic variations. *In*: Stoker, M.S., Evans, D. & Cramp, A. (eds) *Geological Processes on Continental Margins: Sedimentation, Mass-wasting and Stability*. Geological Society, London, Special Publications, **129**, 255–267.

Rasmussen, T.L., Thomsen, E., van Weering, T.C.E. & Labeyrie, L. 1996. Rapid changes in surface and deep water conditions at the Faeroe Margin during the last 58,000 years. *Paleoceanography*, **11**, 757–771.

RAYMO, M.E., OPPO, D.W. *ET AL.* 2004. Stability of North Atlantic water masses in face of pronounced climate variability during the Pleistocene. *Paleoceanography*, **19**, PA2008, doi: 10.1029/2003PA000921.

SZÉRÉMÉTA, N., BASSINOT, F., BALUT, Y., LABEYRIE, L. & PAGEL, M. 2004. Oversampling of sedimentary series collected by giant piston corer: Evidence and corrections based on 3.5-kHz chirp profiles. *Paleoceanography*, **19**, PA1005, doi: 10.1029/2002PA000795.

VAN WEERING, T.C.E., DE HAAS, H., DE STIGTER, H.C., LYKKE-ANDERSEN, H. & KOUVAEV, I. 2003. Structure and development of giant carbonate mounds at the SW and SE Rockall Trough margins, NE Atlantic Ocean. *Marine Geology*, **198**, 67–81.

VOELKER, A.H.L. & WORKSHOP PARTICIPANTS. 2002. Global distribution of centennial-scale records for Marine Isotope Stage (MIS) 3: a database. *Quaternary Science Reviews*, **21**, 1185–1212.

WEAVER, P.P.E. & SCHULTHEISS, P.J. 1990. Current methods for obtaining, logging and splitting marine sediment cores. *Marine Geophysical Researches*, **12**, 85–100.

WEBER, M.E., NIESSEN, F., KUHN, G. & WIEDICKE, M. 1997. Calibration and application of marine sedimentary physical properties using a multi-sensor core logger. *Marine Geology*, **136**, 151–172.

ZOLITSCHKA, B., MINGRAM, J., VAN DER GAAST, S., JANSEN, J.H.F. & NAUMANN, R. 2001. Sediment logging techniques. *In*: LAST, W.M. & SMOL, J.P. (eds) *Tracking Environmental Change Using Lake Sediments. Volume 1: Basin Analysis, Coring, and Chronological Techniques*. Kluwer, Dordrecht, 137–153.